Control of spin configuration in half-metallic $La_{0.7}Sr_{0.3}MnO_3$ nano-structures

J. Rhensius,[1,2,3] C. A. F. Vaz,[1,a)] A. Bisig,[1,3] S. Schweitzer,[3] J. Heidler,[1] H. S. Körner,[1,3] A. Locatelli,[4] M. A. Niño,[4] M. Weigand,[5] L. Méchin,[6] F. Gaucher,[6] E. Göring,[7] L. J. Heyderman,[2] and M. Kläui[1,3]

[1)] *SwissFEL, Paul Scherrer Institut, 5232 Villigen PSI, Switzerland & Laboratory for Nanomagnetism and Spin Dynamics, Ecole Polytechnique Fédérale de Lausanne (EPFL), 1015 Lausanne, Switzerland*

[2)] *Laboratory for Micro- and Nanotechnology, Paul Scherrer Institut, 5232 Villigen PSI, Switzerland*

[3)] *Fachbereich Physik, Universität Konstanz, Universitätsstraße 10, D-78457 Konstanz, Germany*

[4)] *Sincrotrone Trieste, 34149 Basovizza-Trieste, Italy*

[5)] *Helmholtz-Zentrum Berlin für Materialien und Energie GmbH, 12489 Berlin, Germany*

[6)] *Université de Caen Basse-Normandie and CNRS, UMR 6072 GREYC, F-14032 Caen, France & ENSICAEN, UMR 6072 GREYC, F-14050 Caen, France*

[7)] *Max-Planck-Institut für Metallforschung, Heisenbergstrasse 3, 70569 Stuttgart, Germany*

(Dated: 11 May 2011)

We investigate the interplay between the governing magnetic energy terms in patterned $La_{0.7}Sr_{0.3}MnO_3$ (LSMO) elements by direct high-resolution x-ray magnetic microscopy as a function of temperature and geometrical parameters. We show that the magnetic configuration evolves from multidomain to flux-closure states (favored by shape anisotropy) with decreasing element size, with a thickness-dependent crossover at the micrometer scale. The flux-closure states are stable against thermal excitations up to near the Curie temperature. Our results demonstrate control of the spin state in LSMO elements by judicious choice of the geometry, which is key for spintronics applications requiring high spin-polarizations and robust magnetic states.

[a)]Corresponding author. Email: carlos.vaz@cantab.net

Half-metals are characterized by one semiconducting and one metallic spin band, rendering the conduction electrons fully spin-polarized at the Fermi level. This property makes this class of materials ideally suited for applications such as spin-injectors for spintronics devices and magnetic random access memory elements based on the tunnel magnetoresistance effect.[1] The optimally doped $La_{0.7}Sr_{0.3}MnO_3$ (LSMO) is a half-metal with a measured spin polarization of nearly 100%,[2] and a critical temperature $T_c \approx 370$ K,[3] making it a good candidate for room temperature device applications.[4,5] LSMO belongs to a class of compounds known as the "colossal" magnetoresistance (CMR) manganites, which are characterized by a rich electronic behavior as a function of chemical doping, strain, and magnetic and electric fields. This sensitivity to external parameters makes the CMR manganites particularly suited for studying a wide range of physical phenomena, including the role of charge carrier density on the spin configuration in multiferroic heterostructures[6,7] and metal to insulator transition,[8] and the role of strain on the equilibrium magnetic state.[9] The study of static and dynamic properties of domains and in particular of domain walls in this class of materials is also of interest for applications in mass storage concepts based on domain walls,[10,11] while the high spin polarization P together with low saturation magnetization M_s at temperatures near T_c promise a high spin-torque efficiency for current-induced domain wall motion (which scales as P/M_s).[12] For the realization of experiments and applications based on single domains or domain walls, one needs a suitable system with controllable domain states. This is best accomplished in systems with low magnetocrystalline anisotropies, where the spin configuration can be controlled by shape anisotropy. However, so far, high spin polarization materials such as Fe_3O_4 and CrO_2 have shown spin structures that are strongly dominated by magnetocrystalline anisotropies,[13,14] which makes them unsuitable for many devices. In this Letter, we study the evolution of the magnetic states of highly spin polarized LSMO thin film elements as a function of size, shape, thickness, and temperature to show that for sufficiently small elements the equilibrium states consist of flux closure states, which are stable up to T_c. Well defined domain walls arise in confined structures, demonstrating that the spin structure can be tailored by the element geometry, making it an ideal candidate for spintronic applications, such as spin-torque based devices.

The LSMO films (15 nm and 50 nm in thickness) were deposited by pulsed laser deposition from a stoichiometric target onto $SrTiO_3(001)$ single crystal substrates. The laser radiation energy of the KrF excimer laser (248 nm) was 220 mJ at a repetition rate of 3 Hz. The

oxygen pressure was 0.35 mbar and the substrate temperature was held at 720°C during growth. These parameter values were found optimal for producing single-crystalline films with smooth surfaces as judged by X-ray diffraction (XRD) and atomic force microscopy (AFM). The XRD results confirm that the LSMO films are [001]-oriented, while SQUID magnetometry shows that the magnetization is in-plane, with a Curie temperature of about 340 K (see Fig. 2), typical for good quality films of this composition. The micro- and nano-patterning was carried out with focused ion beam (FIB) lithography, where a focused Ga ion beam induces local structural changes and Ga implantation, driving the LSMO to a non-magnetic state. This effect is used to pattern microscopic structures, by writing non-ferromagnetic lines to define the borders of the element.

X-ray circular magnetic dichroism (XMCD) imaging was performed in order to study the (in-plane) spin configuration of patterned LSMO thin films. Two methods are used, both based on the absorption of circularly polarized photons at the Mn L_3-edge: (i) scanning total electron yield microscopy, where a focused X-ray beam generates photoelectrons that are counted for each scanned pixel, a newly developed technique[15] which is well suited for imaging small regions with a high resolution; (ii) photoemission electron microscopy (PEEM),[16] used to image larger areas of the patterned film. XMCD images were taken on different element geometries for 15 nm and 50 nm thick LSMO films, after magnetizing the samples with a strong initial magnetic field $\mathbf{B}_{\mathrm{Init}}$ of $\sim$1 kG.

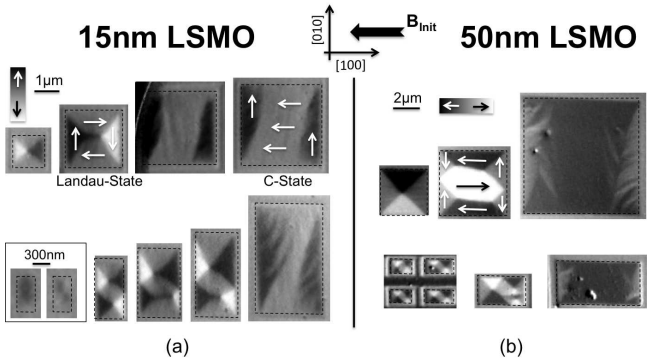

FIG. 1. XMCD images of patterned LSMO microstructures, (a) 15 and (b) 50 nm in thickness (300 K). The paramagnetic boundary delineating the elements appears as gray (the borders of the magnetic elements are indicated by dashed lines).

The evolution of the magnetic state as a function of element size shows a transition from

a multidomain state to simpler, shape anisotropy-dominated, magnetic states with decreasing lateral dimension. This is illustrated in Fig. 1 for square and rectangle elements (and in Fig. 3(b) for disc elements). The larger elements have a domain configuration similar to a high moment C-state, but with domains not uniformly magnetized (with ripple contrast) separated by irregular domains walls, which we associate with local pinning of the magnetization that may help stabilize these high magnetic moment configurations. For lateral dimensions below about 2 μm and 4 μm for the 15 nm and 50 nm thick LSMO films, respectively, the magnetic states fall into well-defined shape anisotropy-dominated flux closure states, with uniformly magnetized domains and sharp domain walls. This shows that at sufficiently small sizes, the magnetostatic energy dominates the micromagnetic configuration of the system and, in particular, that the strength of the pinning sites is smaller than the magnetostatic energy. That epitaxial LSMO thin films are magnetically soft down to the submicrometer scale, a key prerequisite for use in devices, is an unexpected result, given the presence of epitaxial strain (which tends to introduce strong pinning), and the tendency of these complex oxides to phase segregate.[17] While in epitaxial 3d metals the magnetocrystalline anisotropy and pinning often dominate, here we find a soft magnetic behavior reminiscent of the softer polycrystalline 3d metal structures, but in an epitaxial high spin polarization material. For the smallest elements (300 nm $\times$ 500 nm rectangles), one observes the transition to quasi-uniform states for the 15 nm LSMO elements, indicating that at this thickness the exchange energy cost associated with the presence of domain walls becomes larger than the magnetostatic energy.

For the 15 nm thick LSMO elements, the Landau states shown in Fig. 1(a) are found to be slightly distorted, with [100]-oriented domains larger than [010] domains. This is interpreted as arising from the presence of a small uniaxial anisotropy contribution, which sets a preferred orientation of the magnetization (confirmed by SQUID magnetometry). The influence of the uniaxial anisotropy can also be seen in the 50 nm thick sample, where the anisotropy slightly favors [100] domains in the flux closure pattern. AFM data of LSMO films on STO show the existence of steps, which are expected to induce a magnetic uniaxial anisotropy.[18–20] The step density in our films is low compared to the films investigated in Refs. 18–20, resulting in a small anisotropy contribution and explaining the dominant role of the shape anisotropy in our elements. The tuning of the magnetic anisotropy by appropriately engineering the substrate is then an additional degree of freedom that can be

used to control the magnetic state.[19–21]

The thermal stability of the magnetic states was studied by imaging the magnetic states as function of temperature to above T_c. The result of one such measurement for a Landau state in a 50 nm thick LSMO square element is shown in Fig. 2. In order to show that a lack of XMCD contrast corresponds to a non-magnetic state, we compare the XMCD contrast with the results of SQUID magnetization measurements, confirming that for temperatures above 340 K the system is in a paramagnetic state (ruling out that the lack of magnetic contrast in PEEM is related to limitations in spatial or temporal resolution). The images in Fig. 2 show that the Landau state persists up to ∼340 K, and is recovered upon cooling from above T_c, demonstrating that the low energy states are thermally stable up temperatures close to T_c, which is necessary for spin torque experiments that entail Joule heating. Multidomain states, on the other hand, tend to change with increasing temperature and are not reproduced upon cooling.

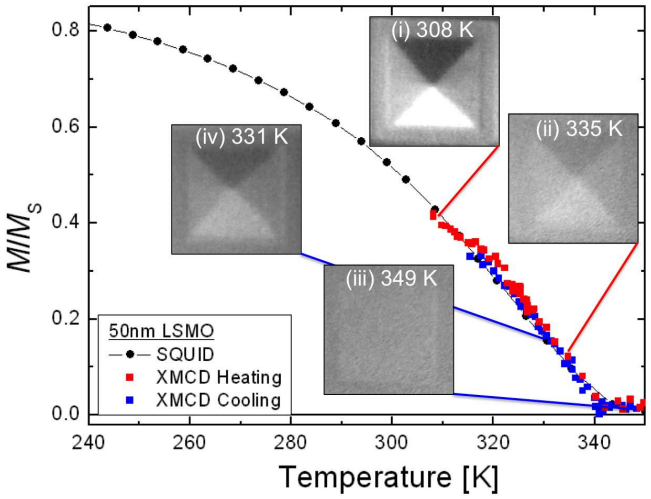

FIG. 2. (Colour online) Scaled XMCD contrast vs temperature for a 50 nm LSMO square element, 3.3 μm size (red squares for heating and blue squares for cooling) and SQUID magnetometry measurements (circles), used to calibrate the temperature scale for the XMCD data. The inset shows XMCD images of the domain states at (i) 308 K, (ii) 335 K, (iii) 349 K, and (iv) 331 K in the cooling cycle.

Ring elements were used as prototypical structures for the study of domain walls in confined LSMO structures.[22] In Fig. 3 we present magnetic images of ring elements with widths in the range from 0.2-2.2 μm. One finds that the rings are in the so-called 'onion'

state, corresponding to the presence of two domains in a ring, separated by two domain walls. A scanning total electron yield XMCD image of a 15 nm thick LSMO ring, 650 nm in width, is shown in Fig. 3(a). For this particular ring dimension, vortex domain walls (short black and white arrows) separate the two domains of the onion state (long black arrows). Fig. 3(b) shows ring elements with widths ranging from 600 nm (II) up to 2.2 μm (III) for the 50 nm thick LSMO film; the rings favor the formation of vortex walls, although double vortex walls are also observed, as in Fig. 3(b)(IV) (domain wall to the right). These results demonstrate that by tuning the size and geometry of the element, one is able to control the type of domain wall present in a confined geometry. The magnetic configurations found in our structures can be reproduced well by micromagnetic simulations,[23] showing that the spin structure in LSMO can be controlled by a suitable choice of the element geometry and that the relevant spin structures, such as well-defined domain walls, can be selectively positioned and controlled in this material, which is a key step to using this material in a device. These results indicate that LSMO follows similar micromagnetic energetics as 3d ferromagnetic elements,[22] and have the advantage of not only having well-controlled spin structures but also the high spin polarization of a half-metal.

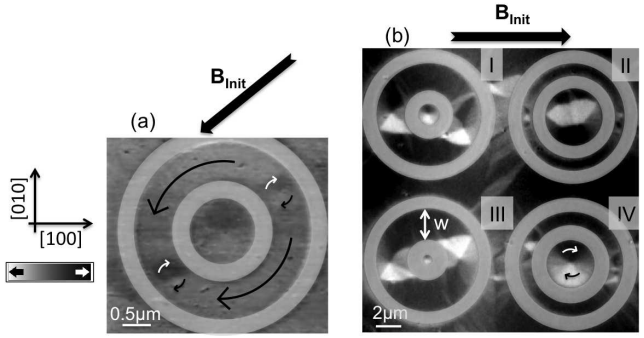

FIG. 3. XMCD images of LSMO rings and discs after saturation (300 K). (a) XMCD-TEY image of a 15 nm LSMO/STO ring, 620 nm in width, and of a 1.2 μm diameter disc in the center. An onion state is present in the ring, with vortex walls separating the two domains. The central disc is in the vortex state. (b) XMCD image of 50 nm LSMO ring and disc elements. (To guide the eye, the nonmagnetic area is grayed out.)

In summary, we have determined the dimensional crossover from multidomain to shape-defined magnetic states in highly spin-polarized LSMO structures. Weak pinning and low

magnetic anisotropies give rise to highly symmetric states that are determined by the shape anisotropy. In particular, we show that well defined domain walls are generated in spatially confined geometries such as rings, whose character can be controlled by varying the width of the element. In addition, we demonstrate that the low energy states are robust against thermal excitation up to the critical temperature. These results show that LSMO is a promising candidate for both the study of fundamental domain wall phenomena in highly spin polarized materials and for device applications, where robust and well determined spin configurations are key.

We would like to thank M. Hagner for support with sample preparation. This work was funded by EU's 7th Framework Programme IFOX NMP3-LA-2010-246102.

REFERENCES

[1]H. Hidaka, in *Embedded Magnetic RAM*, edited by K. Zhang (Springer-Verlag, 2009) p. 241.

[2]J.-H. Park, E. Vescovo, H.-J. Kim, C. Kwon, R. Ramesh, and T. Venkatesan, Nature **392**, 794 (1998).

[3]G. H. Jonker and J. H. van Santen, Physica **16**, 337 (1950).

[4]C. A. F. Vaz, C. H. Ahn, and V. E. Henrich, in *Spin-polarisation effects in oxide materials*, edited by A. Hirohata and Y. Otani (Research Signpost, 2009) p. 145.

[5]J. Cibert, J.-F. Bobo, and U. Lüders, C. R. Physique **6**, 977 (2005).

[6]H. J. A. Molegraaf, J. Hoffman, C. A. F. Vaz, S. Gariglio, D. van der Marel, C. H. Ahn, and J.-M. Triscone, Adv. Mater. **21**, 3470 (2009).

[7]C. A. F. Vaz, J. Hoffman, Y. Segal, J. W. Reiner, R. D. Grober, Z. Zhang, C. H. Ahn, and F. J. Walker, Phys. Rev. Lett. **104**, 127202 (2010).

[8]X. Hong, A. Posadas, A. Lin, and C. H. Ahn, Phys. Rev. B **68**, 134415 (2003).

[9]Y. Wu, Y. Matsushita, and Y. Suzuki, Phys. Rev. B **64**, 220404(R) (2001).

[10]R. Cowburn, U.S. Patent No. WO/2007/132174.

[11]S. S. P. Parkin, M. Hayashi, and L. Thomas, Science **320**, 190 (2008).

[12]A. Thiaville, Y. Nakatani, J. Miltat, and Y. Suzuki, Europhys. Lett. **69**, 990 (2005).

[13]A. Biehler, M. Kläui, M. Fonin, C. König, G. Güntherodt, and U. Rüdiger, Phys. Rev. B **75**, 184427 (2007).

[14]M. Fonin, C. Hartung, U. Rüdiger, D. Backes, L. Heyderman, F. Nolting, A. F. Rodríguez, and M. Kläui, J. Appl. Phys. **109**, 07D315 (2011).

[15]E. Göring *et al.*, unpublished (2011).

[16]J. Stöhr, Y. Wu, B. D. Hermsmeier, M. G. Samant, G. R. Harp, S. Koranda, D. Dunham, and B. P. Tonner, Science **258**, 658 (1993).

[17]E. Dagotto, Science **309**, 257 (2005).

[18]M. Mathews, F. M. Postma, J. C. Lodder, R. Jansen, G. Rijnders, and D. H. A. Blank, Appl. Phys. Lett. **87**, 242507 (2005).

[19]M. Kubota, T. Taniuchi, R. Yasuhara, H. Kumigashira, M. Oshima, K. Ono, H. Okazaki, T. Wakita, T. Yokoya, H. Akinaga, M. Lippmaa, M. Kawasaki, and H. Koinuma, Appl. Phys. Lett. **91**, 182503 (2007).

[20]Y. Takamura, R. V. Chopdekar, A. Scholl, A. Doran, J. A. Liddle, B. Harteneck, and Y. Suzuki, Nano Letters **6**, 1287 (2006).

[21]P. Perna, L. Méchin, M. Saïb, J. Camarero, and S. Flament, New J. Phys. **12**, 103033 (2010).

[22]M. Kläui, J. Phys.: Condens. Matter **20**, 313001 (2008).

[23]http://math.nist.gov/oommf/.

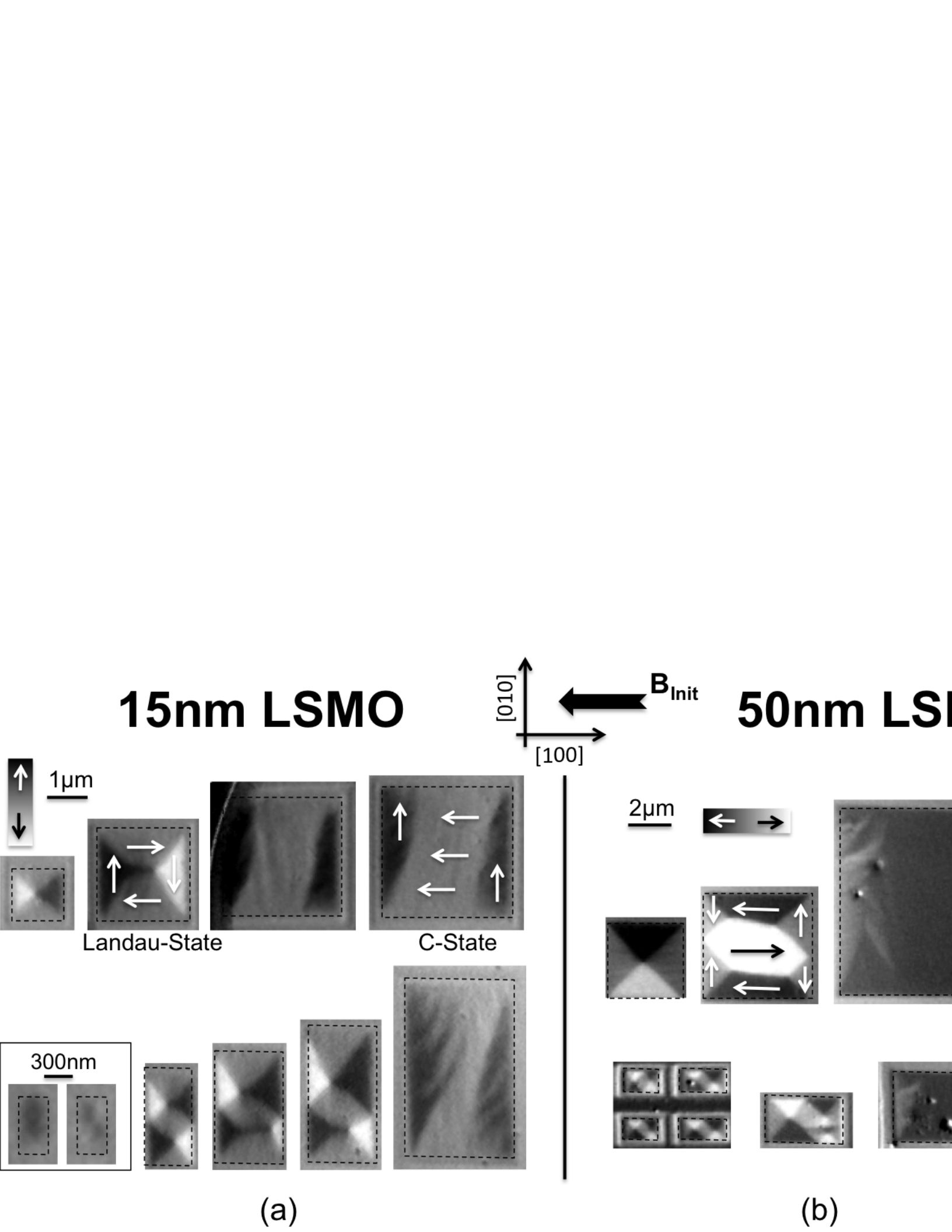
15nm LSMO
[010]
[100]
B Init
50nm LS
1µm
Landau-State
C-State
300nm
2µm
(a)
(b)

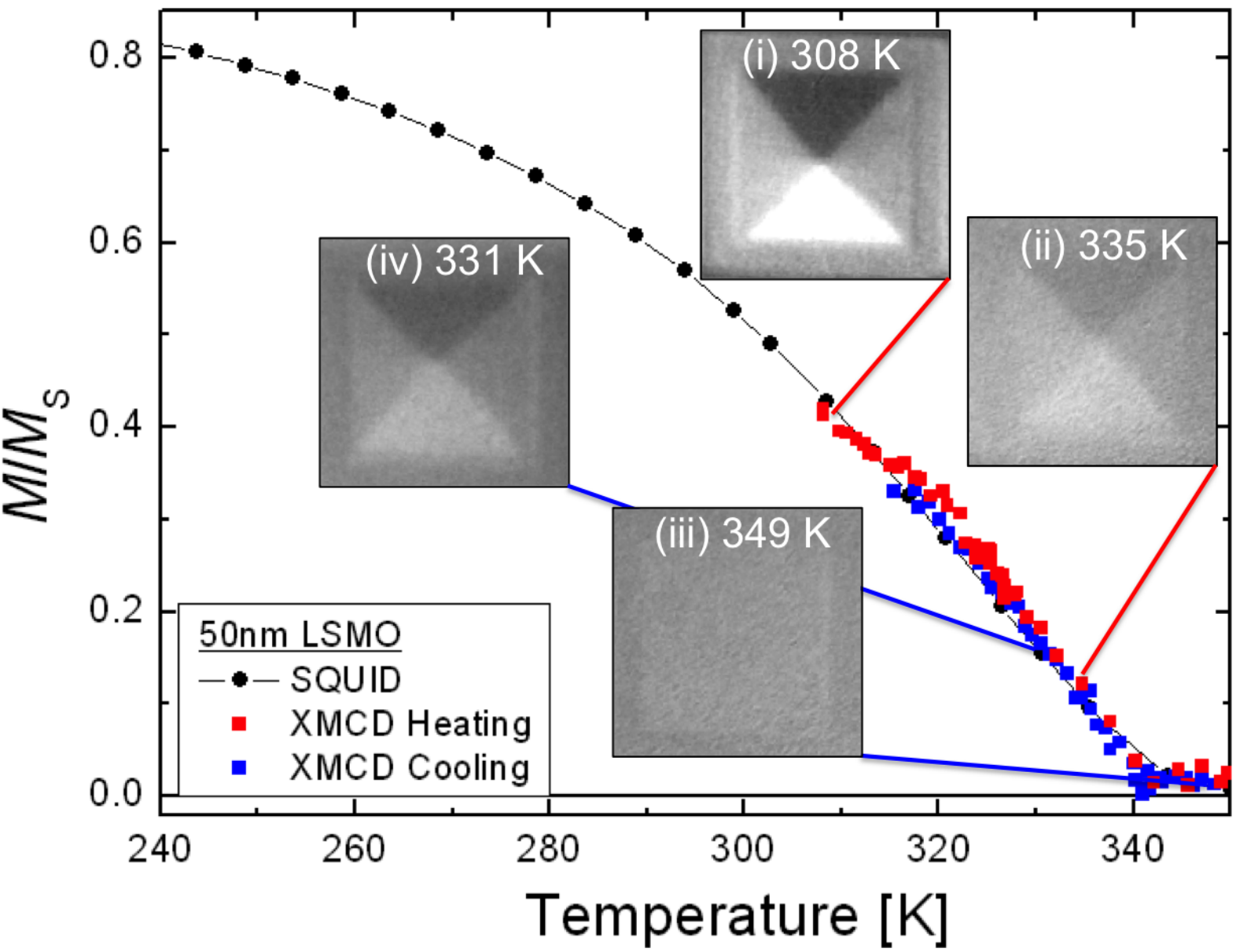
0.8
0.6
0.4
0.2
0.0
M/M_S
240
260
280
300
320
340
Temperature [K]
(i) 308 K
(ii) 335 K
(iii) 349 K
(iv) 331 K
50nm LSMO
SQUID
XMCD Heating
XMCD Cooling

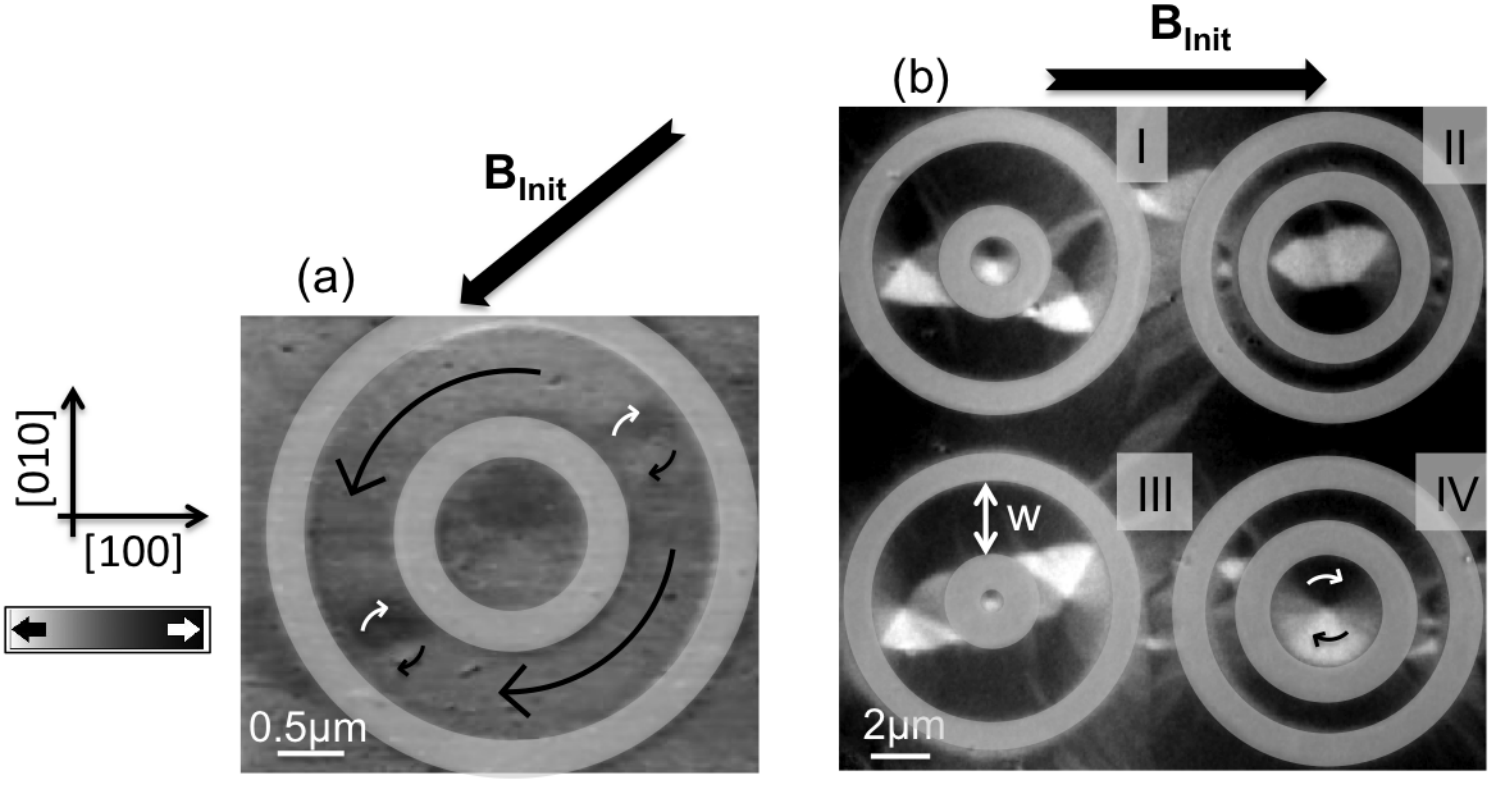
(a)
B_Init
[010]
[100]
0.5µm
(b)
B_Init
I
II
III
IV
w
2µm